Medical Physics
The International Journal of Medical Physics Research and Practice

Compressed sensing for longitudinal MRI: An adaptive-weighted approach

Lior Weizman, Yonina C. Eldar, and Dafna Ben Bashat

Citation: Medical Physics **42**, 5195 (2015); doi: 10.1118/1.4928148
View online: http://dx.doi.org/10.1118/1.4928148
View Table of Contents: http://scitation.aip.org/content/aapm/journal/medphys/42/9?ver=pdfcov
Published by the American Association of Physicists in Medicine

Compressed sensing for longitudinal MRI: An adaptive-weighted approach

Lior Weizman[a] and Yonina C. Eldar
Department of Electrical Engineering, Technion - Israel Institute of Technology, Haifa 32000, Israel

Dafna Ben Bashat
Functional Brain Center, Tel Aviv Sourasky Medical Center, Sackler Faculty of Medicine and Sagol School of Neuroscience, Tel Aviv University, Tel Aviv 64239, Israel

(Received 6 January 2015; revised 19 July 2015; accepted for publication 25 July 2015; published 11 August 2015)

Purpose: Repeated brain MRI scans are performed in many clinical scenarios, such as follow up of patients with tumors and therapy response assessment. In this paper, the authors show an approach to utilize former scans of the patient for the acceleration of repeated MRI scans.
Methods: The proposed approach utilizes the possible similarity of the repeated scans in longitudinal MRI studies. Since similarity is not guaranteed, sampling and reconstruction are adjusted during acquisition to match the actual similarity between the scans. The baseline MR scan is utilized both in the sampling stage, via adaptive sampling, and in the reconstruction stage, with weighted reconstruction. In adaptive sampling, *k*-space sampling locations are optimized during acquisition. Weighted reconstruction uses the locations of the nonzero coefficients in the sparse domains as a prior in the recovery process. The approach was tested on 2D and 3D MRI scans of patients with brain tumors.
Results: The longitudinal adaptive compressed sensing MRI (LACS-MRI) scheme provides reconstruction quality which outperforms other CS-based approaches for rapid MRI. Examples are shown on patients with brain tumors and demonstrate improved spatial resolution. Compared with data sampled at the Nyquist rate, LACS-MRI exhibits signal-to-error ratio (SER) of 24.8 dB with undersampling factor of 16.6 in 3D MRI.
Conclusions: The authors presented an adaptive method for image reconstruction utilizing similarity of scans in longitudinal MRI studies, where possible. The proposed approach can significantly reduce scanning time in many applications that consist of disease follow-up and monitoring of longitudinal changes in brain MRI. [http://dx.doi.org/10.1118/1.4928148]

Key words: rapid MR, compressed sensing, longitudinal studies

1. INTRODUCTION

Repeated brain MRI scans are performed in many clinical scenarios, such as follow up of patients with tumors and therapy response assessment.[1–5] They constitute one of the most efficient tools to track pathology changes and to evaluate treatment efficacy in brain diseases. In many cases, most of the imaging data of the repeated scan are already present in the former scan. In this paper, we aim at exploiting this temporal similarity in MRI longitudinal studies for rapid MRI acquisition of the repeated scan.

The use of a reference image in medical image reconstruction is quite established and is popular in various imaging modalities. Examples include computed tomography,[6,7] spectroscopic imaging,[8] imaging of contrast agent uptake,[9] dynamic MRI (Refs. 10–15) and real time tracking of tumors,[4] locally focused MRI,[16] and feature-recognizing MRI.[17]

Since the introduction of compressed sensing (CS)[18–21] to the field of MRI,[22] the use of a reference image has been exploited within CS, such as in rapid dynamic MRI, by exploiting temporal sparsity. Gamper *et al.* perform randomly skipping phase-encoding lines in each dynamic frame to speed-up acquisition.[23] Liang *et al.* propose an iterative algorithm to detect the signal support in CS dynamic MRI.[24] Zonoobi and Kassim use the previous time-frame in dynamic MRI to weight the ℓ_1 minimization in the CS reconstruction process.[25] Trzasko *et al.* exploit a preinjection background image[26] and Wu *et al.* utilize a constraining image to enhance MR angiography (MRA), while incorporating CS and parallel imaging.[27]

Samsonov *et al.*[28] suggested using a reference frame to speed-up MRI in longitudinal studies. Their approach, as well as most other techniques that exploit a reference image in MRI applications, relies on similarity between the reference scan and the current scan. The similarity assumption is indeed valid in cases where imaging data consist of many images acquired at a high frame rate.

However, longitudinal MRI poses a different challenge due to the large time gaps between the scans. On the one hand, similarity across time points is not guaranteed, since in many cases, we observe vast changes between scans due to pathology changes or surgical interventions. In addition, undersampling in the time domain is impractical, due to the demand for high quality reconstruction at each time point. Therefore, reconstruction errors in this single time-frame imaging modality cannot be compensated for by adjacent time-frames like in dynamic imaging. On the other hand, in cases where similarity between previous and current scans does exist, the high resolution former scan of the patient may constitute a very strong

prior for the reconstruction of the repeated scan. Therefore, for the scenario of longitudinal MRI, we suggest exploiting the former scan in an adaptive manner. The similarity of the reference scan to the current scans is "learned" during the acquisition process, leading to an iterative update of sampling and reconstruction accordingly.

In the context of MRI, image reconstruction quality highly depends on the k-space sampling pattern.[29,30] The concept of adaptive sampling (also known as "adaptive sensing") suggests that samples are selected sequentially, where the choice of the next samples may depend on previously gathered information. This concept has been implemented previously, mainly for dynamic MRI,[31,32] and was later extended and implemented in a CS framework.[33–35] In this work, we utilize this concept and explore whether we can adaptively optimize the sampling pattern on-the-fly, based on partial reconstruction results from previously acquired samples in longitudinal MRI.

A substantial body of mathematical theory has recently been published establishing the basic principles of adaptive sampling of sparse signals.[36–38] According to these mathematical results, reconstruction from samples selected sequentially based on partial reconstruction results can be significantly better than reconstruction from nonadaptive (deterministic or random) samples.

Knowledge of the former scan may be advantageously used not only to design an adaptive sampling pattern but also to improve image reconstruction from sampled data. This improvement can be obtained via the definition of regularization weights in the reconstruction optimization problem.[39–41] We apply this approach, coined "weighted reconstruction," for the scenario of longitudinal MRI. This weighting mechanism allows to relax or enforce the demand for sparsity according to the level of similarity between the current scan and the reference scan.

In this paper, we develop a framework for CS longitudinal MRI, by employing the two well established approaches above in parallel: adaptive sampling and weighted reconstruction. In this way, we exploit the prior scan of the patient to reconstruct the repeated scan from highly undersampled k-space data. To keep the discussion as simple as possible, we focus on Cartesian sampling for brain MRI.

The novelty of this paper lies in the unique implementation of weighted reconstruction and adaptive sampling for the scenario of longitudinal studies, where the temporal similarity is not taken for granted. Unlike traditional CS MRI approaches that utilize prior constraints, in our approach, the temporal similarity assumption is continuously examined, and the sampling and reconstruction algorithms are updated accordingly. Experimental results demonstrate the superiority of the proposed method regardless of the validity of the temporal similarity assumption in the examined cases.

This paper is organized as follows. Section 2 presents the theory of weighted reconstruction and adaptive sampling and their implementation for longitudinal MRI. Section 3 describes the experimental results. Section 4 discusses practical issues related to implementation of the method in real time applications; Sec. 5 concludes by highlighting the key findings.

2. METHOD

2.A. Summary of compressed sensing MRI

The application of CS for rapid MRI (Ref. 22) exploits the fact that MRI scans are typically sparse in some transform domain, which is incoherent with the sampling domain. Nonlinear reconstruction is then used to enforce both sparsity of the image representation and consistency with the acquired data. A typical formulation of CS MRI recovery aims to solve the following constrained optimization problem:

$$\min_{\mathbf{x}} \quad \|\mathbf{\Psi x}\|_1 \ \text{ such that } \quad \|\mathbf{F}_u\mathbf{x}-\mathbf{y}\|_2 < \epsilon, \tag{1}$$

where $\mathbf{x} \in \mathbb{C}^N$ is the N-pixel complex image to be reconstructed, represented as a vector, $\mathbf{y} \in \mathbb{C}^M$ represents the k-space measurements, $\mathbf{F}_u$ is the undersampled Fourier transform operator, $\mathbf{\Psi}$ is a sparsifying transform operator, and ϵ controls the fidelity of the reconstruction to the measured data.

This fundamental CS MRI formulation is the basis for many MRI reconstruction applications, where the sparse transform domain varies depending on the particular setting. In MR angiography, where images are truly sparse, finite-differences are used as a sparsifying transform. In dynamic MRI, the difference between adjacent time frames is sparse.[23,42,43] Sparsity can also be exploited in multiple domains, for example, in both temporal and spatial domains.[44]

Here, we focus on Cartesian sampling, so that $\mathbf{F}_u$ represents line samples of the k-space in 2D imaging. We further consider brain MRI, known to be sparse in the wavelet domain. Therefore, we will assume throughout that $\mathbf{\Psi}$ is an appropriately chosen wavelet transform.

2.B. The sparsity of longitudinal MRI scans

In longitudinal studies, patients are scanned every several weeks or months. This scanning scheme is broadly used, for follow-up purposes and for therapy response assessment. In this setting, we could save scanning time if we are able to scan only the changes from the baseline. This type of scanning is, of course, not feasible, due to practical difficulties in designing such a sequence and the fact that prior information on the changes is mostly unavailable.

While the scenario of longitudinal studies is fundamentally different from dynamic MRI in many aspects, we still find that similarity across time points often exists. Figure 1 shows an example of the same axial slice taken from multiple scans acquired from a patient with optic pathway glioma (OPG), demonstrating a relatively slow growing tumor pattern. The bottom row of the figure shows the representation of each time point in the Daubechies-4 wavelet transform,[45] which is widely used as a sparse transform for brain MRI. The similarity between image slices acquired at several time points is clearly demonstrated. Moreover, the representation of the images in the wavelet domain is sparse, and the locations of the dominant wavelet coefficients (also known as the support of the image in the wavelet domain) are similar across the patient's time points.

Exploiting temporal similarity can be embedded in Eq. (1) by an additional term, which will promote sparsity of the

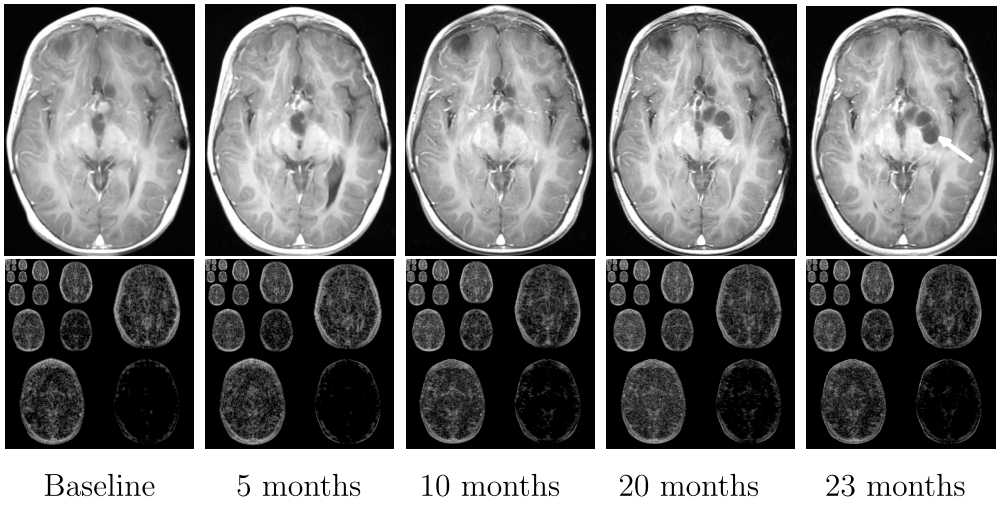

FIG. 1. Brain contrast-enhanced $T1$-weighted longitudinal scans of patient with OPG. The same spatial slice (top) and its representation in the wavelet domain (bottom) are shown before treatment (leftmost image) and 5, 10, 20, and 23 months after the beginning of treatment. It can be seen that despite the cyst evolving over time (marked by an arrow in the rightmost image), many image regions remain unchanged from one time point to another. Moreover, the support of the image in the wavelet domain (bottom) is preserved with no major changes over time.

difference between the image to be reconstructed, $\mathbf{x}$, and a previously acquired image of the same patient, $\mathbf{x}_0$. This leads to the modified problem,

$$\min_{\mathbf{x}} \underbrace{\|\mathbf{\Psi x}\|_1}_{\text{term1}} + \lambda \underbrace{\|\mathbf{x}-\mathbf{x}_0\|_1}_{\text{term2}} \text{ such that } \|\mathbf{F}_u\mathbf{x}-\mathbf{y}\|_2 < \epsilon. \quad (2)$$

Here, term 1 enforces sparsity of $\mathbf{x}$ in the wavelet domain, and term 2 enforces similarity of $\mathbf{x}$ to $\mathbf{x}_0$ in the image domain. The parameter λ trades sparsity in the wavelet domain with sparsity in the temporal domain. This approach of utilizing sparsity in both spatial and temporal domains via CS is coined hereinafter temporal compressed sensing-MRI (TCS-MRI).

Term 2 is sparse if there are no major changes between $\mathbf{x}$ and $\mathbf{x}_0$, both images have similar gray-level intensities and they are spatially matched. While these conditions are met in many applications of dynamic imaging, such as prior image constrained compressed sensing (PICCS) in CT (Refs. 6 and 7) and dynamic MRI,[4,23,43,44] in longitudinal MRI, none of these requirements are guaranteed. Although there are solutions for miss-registration and variable gray-level intensities (see Sec. 4), the temporal similarity in longitudinal MRI is *a priori* unknown. Thus, despite the fact that longitudinal MRI often exhibits temporal similarity,[28] we have to take into account that in many cases, the follow-up scan can be substantially different than the baseline scan. Such cases may occur, for example, if a surgical intervention was applied between the time points or if there is a major progressive or therapy response. Figure 2 shows two representative examples.

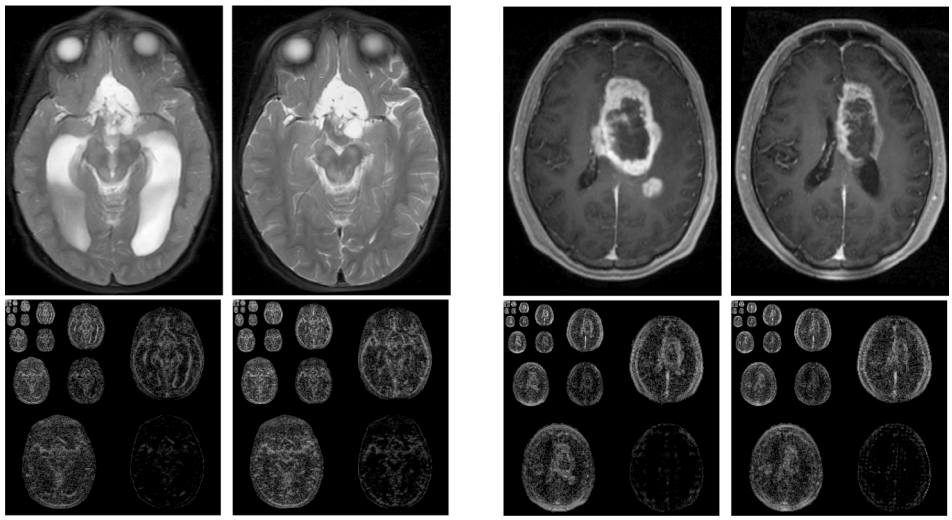

FIG. 2. Left: brain $T2$-weighted consecutive scans of a patient with hydrocephalus. Scans were acquired before and after treatment. Right: contrast-enhanced $T1$-weighted consecutive scans of a patient with glioblastoma multiforme (GBM) acquired during the treatment period. In these cases, there is substantial difference over time between the consecutive scans of the patients, in both the image (top) and the wavelet (bottom) domains.

We conclude that using Eq. (2) for image reconstruction under the assumption of substantial similarity between time points may result in improper reconstruction in cases where this assumption does not hold. To avoid this, we have to carefully design a sampling and reconstruction mechanism that will adjust to match the temporal similarity of the case at hand. To achieve this goal, we extend TCS-MRI using weighted reconstruction and adaptive sampling.

2.C. Adaptive sampling and weighted reconstruction

Many extensions to CS-MRI have been proposed to improve performance of the sampling and reconstruction phases. One of these extensions consists of embedding prior knowledge by weighted reconstruction.[40,41,46–49] Weighted reconstruction can be mathematically embedded into basic CS Eq. (1) by adding a diagonal weighting matrix, $\mathbf{W} = \mathrm{diag}([w_1, w_2, \ldots, w_N])$ as proposed by Candes *et al.*,[39]

$$\min_{\mathbf{x}} \quad \|\mathbf{W}\boldsymbol{\Psi}\mathbf{x}\|_1 \ \text{ such that } \quad \|\mathbf{F}_u\mathbf{x}-\mathbf{y}\|_2 < \epsilon. \tag{3}$$

Here, w_i represents the probability that $i \notin T$, and T is the support of $\mathbf{x}$ in the sparse transform domain. It has been shown that weighted reconstruction outperforms traditional CS-MRI for dynamic MRI,[41,50] where the support of the previous time frame is used as an estimate for the support of the current frame.

Prior knowledge can also be used to optimize the way that data are acquired.[51–53] However, since in longitudinal MRI the similarity between scans is not guaranteed, an adaptive mechanism is needed to determine the level of similarity between scans. Adaptive sampling proposes a selective sample selection, where the choice of the next samples depends on the previously gathered information. It has been proposed to improve signal's support detection from a low number of samples or under a constraint on the total sensing effort.[36,37,54] The rational behind this approach is that the estimation error one can get by using clever sampling based on previously acquired data is generally lower than that achievable by a nonadaptive scheme. While Arias-Castro *et al.*[55] have shown that the validity of this claim is limited in general, it is proven to be valid for many cases.

In MRI, Seeger *et al.*[33] employ this concept to optimize k-space trajectories, by formulating the optimization problem as a Bayesian experimental design problem. They use the posterior uncertainty as the criterion for selecting the next trajectory at each round. Ravishankar and Bresler[34] propose an adaptive scheme that relies on training image scans to optimize the sampling pattern. Their criterion takes into account training data and the reconstruction strategy.

In the application of CS for longitudinal studies, we use weighted reconstruction and adaptive sampling in a "patient-specific" way: k-space trajectories are optimized based on the past scan of the patient currently being scanned and reconstruction is improved via weighted reconstruction. In addition, this approach iteratively detects cases in which the assumption of temporal similarity is not valid and updates the sampling and reconstruction processes accordingly.

2.D. Adaptive-weighted CS for longitudinal MRI

Embedding weighted reconstruction into the longitudinal MRI results in the following minimization problem:

$$\min_{\mathbf{x}} \quad \underbrace{\|\mathbf{W}_1\boldsymbol{\Psi}\mathbf{x}\|_1}_{\text{term1}} + \lambda \underbrace{\|\mathbf{W}_2(\mathbf{x}-\mathbf{x}_0)\|_1}_{\text{term2}} \ \text{ such that } \quad \|\mathbf{F}_u\mathbf{x}-\mathbf{y}\|_2 < \epsilon, \tag{4}$$

where $\mathbf{W}_k$ is a diagonal matrix, $\mathbf{W}_k = \mathrm{diag}([w_k^1, w_k^2, \ldots, w_k^N])$, and w_k^i controls the weight given to each element in the support of term 1 or term 2. Adding $\mathbf{W}_1$ to term 1 relaxes the demand for sparsity on the elements in the support of the image in its sparse transform domain. As a result, sparsity in the wavelet domain is strongly enforced on elements outside of the support. Adding $\mathbf{W}_2$ to term 2 controls the demand for similarity between $\mathbf{x}$ and $\mathbf{x}_0$, enforcing sparsity only in image regions where $\mathbf{x}$ and $\mathbf{x}_0$ are similar.

The solution of problem (4) can be obtained by extending one of the well-known approaches for classical CS.[56,57] In our experiments, we extended the fast iterative shrinkage-thresholding algorithm (FISTA)[58] to solve the unconstrained problem in so-called Lagrangian form,

$$\min_{\mathbf{x}} \quad \|\mathbf{F}_u\mathbf{x}-\mathbf{y}\|_2^2 + \lambda_1 \underbrace{\|\mathbf{W}_1\boldsymbol{\Psi}\mathbf{x}\|_1}_{\text{term1}} + \lambda_2 \underbrace{\|\mathbf{W}_2(\mathbf{x}-\mathbf{x}_0)\|_1}_{\text{term2}}. \tag{5}$$

The values of λ_1 and λ_2 can be selected appropriately such that the solution of Eq. (5) is approximately equal to that of Eq. (4), for a given λ. These values control the trade-off between enforcing sparsity in the wavelet and temporal domains.

When determining the values of $\mathbf{W}_1$ and $\mathbf{W}_2$, we would like to avoid utilizing the prior scan in the reconstruction process if the assumption of similarity between consecutive scans does not hold. More specifically, we design $\mathbf{W}_1$ and $\mathbf{W}_2$ to achieve the following goals:

1. Convergence to CS-MRI Eq. (1) if the assumption of similarity between consecutive scans is not valid (i.e., $w_1^i \to 1$ and $w_2^i \to 0$ if $\mathbf{x}$ and $\mathbf{x}_0$ are significantly different in both image and wavelet domains).
2. Relaxing the demand for sparsity of $\boldsymbol{\Psi}\mathbf{x}$ in regions where $\boldsymbol{\Psi}\mathbf{x}_0$ is not sparse and the similarity assumption between $\boldsymbol{\Psi}\mathbf{x}$ and $\boldsymbol{\Psi}\mathbf{x}_0$ is valid (i.e., $w_1^i \to 0$ as $[|\boldsymbol{\Psi}\mathbf{x}_0|]_i$ grows and images are similar in the transform domain).
3. Relaxing the demand for sparsity of $\mathbf{x}-\mathbf{x}_0$ in regions where the similarity assumption between $\mathbf{x}$ and $\mathbf{x}_0$ is not valid (i.e., $w_2^i \to 0$ as $[|\mathbf{x}-\mathbf{x}_0|]_i$ grows).

To achieve these goals, we first sample N_k k-space samples randomly and reconstruct $\hat{\mathbf{x}}$, which is the estimation of $\mathbf{x}$, by solving Eq. (5) with $\mathbf{W}_1 = \mathbf{I}$ and $\mathbf{W}_2 = \mathbf{0}$. We then sample N_k additional samples and solve Eq. (5) where the elements of the matrices are chosen as follows:

$$w_1^i = \begin{cases} 1, & \dfrac{[|\boldsymbol{\Psi}(\hat{\mathbf{x}}-\mathbf{x}_0)|]_i}{1+[|\boldsymbol{\Psi}(\hat{\mathbf{x}}-\mathbf{x}_0)|]_i} > \epsilon_1 \\ \dfrac{1}{1+[|\boldsymbol{\Psi}\mathbf{x}_0|]_i}, & \text{otherwise} \end{cases}, \tag{6}$$

$$w_2^i = \frac{1}{1+[|\hat{\mathbf{x}}-\mathbf{x}_0|]_i}. \tag{7}$$

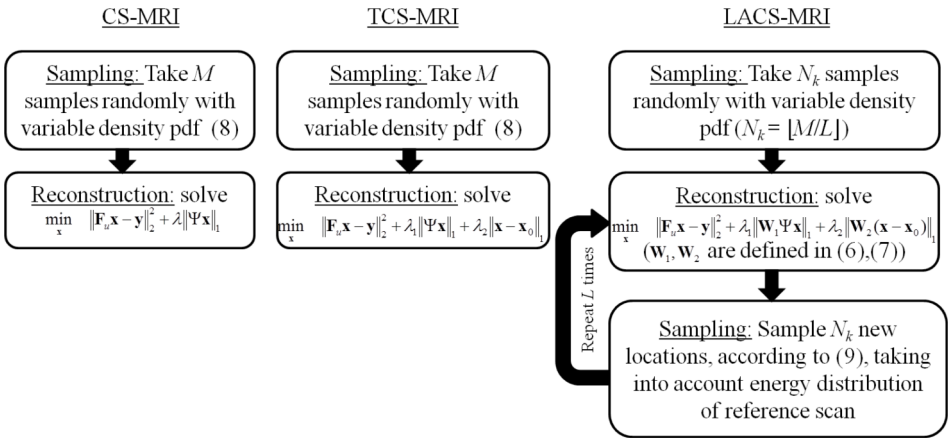

FIG. 3. High-level diagram showing the main steps in CS-MRI, TCS-MRI, and in our proposed adaptive approach, LACS-MRI. All methods acquire M k-space samples. However, in LACS-MRI, only a small portion of the samples is taken from a pure variable density pdf, in the first iteration. The rest of the samples are chosen iteratively, taking into account both the energy distribution of the reference scan, $\mathbf{x}_0$, and variable density pdf.

Here, $[\cdot]_i$ denotes the ith element of the vector in brackets and ϵ_1 is a threshold for defining similarity in the sparse transform domain. This process is repeated until a sufficient number of samples is obtained for adequate recovery. The proposed iterative approach allows exploitation of temporal similarity, when it exists, and prevents degradation of image quality if the consecutive scans are significantly different.

Incorporating adaptive sampling into the longitudinal MRI problem is obtained via adaptive design of the N_k sampling locations at each iteration. It is well known that reconstruction results highly depend on the chosen sampling trajectories in the k-space domain. For instance, experiential results have shown that it is desirable to undersample less near the k-space origin and more in the periphery of the k-space.[22,29] A common sampling scheme is variable density random undersampling (VDS), which can be implemented by choosing samples randomly with sampling density scaling according to a power of distance from the origin.

For simplicity, we assume that 2D Cartesian sampling is used, and N_k is the number of rows in the k-space domain. To utilize VDS in 2D Cartesian sampling, we define the discrete polynomial distribution as

$$f_{\mathrm{VD}}(k_y) = \frac{\left(1-\frac{2}{N_k}|k_y|\right)^p}{\sum_{k_y}\left(1-\frac{2}{N_k}|k_y|\right)^p}, \tag{8}$$

where $-(N_k/2) < k_y \le N_k/2$ denotes the k-space coefficients in the phase encoding direction and p is the power distance from the origin.

VDS is used as the probability density function (pdf) for random sampling in many cases where the real distribution of the data is *a priori* unknown. However, in longitudinal studies, we may rely on the reference scan data distribution, if scans are similar. Inspired by Chen *et al.*,[38] our adaptive approach will converge to random sampling according to the reference scan data pdf if it is similar to the follow-up scan, and to polynomial pdf otherwise. Therefore, samples in our approach are taken randomly using the following pdf:

$$f_S(k_y) = \gamma f_B(k_y) + (1-\gamma) f_{VD}(k_y), \tag{9}$$

where f_B is the pdf of the baseline's phase encode lines' energy, defined as

$$f_B(k_y) = \frac{g_B(k_y)}{\sum_{k_y} g_B(k_y)}, \qquad g_B(k_y) = \sum_{i\in k_y} [|\mathbf{F}\mathbf{x}_0|]_i, \tag{10}$$

where $\mathbf{F}$ indicates the $N\times N$ Fourier matrix, $[\cdot]_i$ denotes the ith element of the vector in brackets, and γ is the fidelity we give to the similarity between the current and the previous scan. Since $\mathbf{W}_2$ can serve as a good approximation for this similarity, γ is computed as its mean over the main diagonal: $\gamma = 1/N\sum_{i=1}^{N} w_2^i$.

A diagram presenting the major differences between CS-MRI, TCS-MRI, and the proposed method is shown in Fig. 3. Implementation details of our algorithm can be found in our technical report.[59] This scheme for longitudinal adaptive-weighted compressed sensing is coined hereinafter longitudinal adaptive compressed sensing MRI (LACS-MRI).

3. EXPERIMENTAL RESULTS

3.A. Experimental settings

Our experiments consist of repeated scans of pomelo and patients with OPG and glioblastoma multiforme (GBM). The patients with OPG were scanned with a GE Signa 1.5 T HDx scanner and the pomelo and GBM experiments were performed on a GE Signa 3 T HDXT scanner. In our experiments, partial k-space acquisition was obtained by down-sampling, in a software environment, a fully sampled k-space. All CS reconstructions were implemented in MATLAB (The MathWorks, Natick, MA). We compare our approach (LACS-MRI) with two nonadaptive schemes, CS-MRI and TCS-MRI. CS-MRI is described in Ref. 22 and TCS-MRI takes into account the knowledge of the prior scan in the time sequence, by solving Eq. (2) for image reconstruction.

In our experiments, we used the Daubechies 4 wavelet transform. Reconstructions based on nonadaptive sampling (CS-MRI and TCS-MRI) were obtained with variable density undersampling. Since we do not know the distribution of the data in the k-space domain, we used the state-of-the-art variable density undersampling scheme considered in many

applications of CS for MRI.[22,33] In this scheme, samples were taken randomly according to the pdf in Eq. (8) with $p = 4$. In 2D Cartesian sampling, 5% of the phase encode lines, located in the center of the k-space, were acquired in full. In 3D Cartesian sampling, 1% of the central phase encode plane was acquired in full. For LACS-MRI, we used the same variable density random pattern for the first iteration, while subsequent samples were taken according to our adaptive sampling approach with the pdf in Eq. (9).

LACS-MRI and TCS-MRI ℓ_1-minimization problems were solved in their Lagrangian form using the FISTA algorithm.[58] CS-MRI was tested both with our FISTA-based implementation of solving Eq. (1) and with the nonlinear conjugate subgradient algorithm as described in Lustig *et al.*,[22] which adds a total variation (TV)[60] penalty to Eq. (1), where the best results (in terms of resolution improvement) are shown. The threshold for defining similarity in the sparse transform domain was set to $\epsilon_1 = 0.1$. In all experiments, different values of λ_1, λ_2 in the range of [0.001,0.9] were examined, and the best result is shown for each reconstruction algorithm.

For quantitative evaluation, the signal-to-error ratio (SER) is computed for each reconstruction result, as $\mathrm{SER} = 10\log_{10}(\sigma_{\mathbf{x}}/V_s)$, where $\sigma_{\mathbf{x}}$ denotes the variance of the values in $\mathbf{x}$ and V_s is the mean squared-error (MSE) between the original image, $\mathbf{x}$ and the reconstructed image, $\hat{\mathbf{x}}$. Note that in some cases, clinical decisions are based on subtle changes between the baseline and the follow-up scans, which are not reflected in SER. Therefore, results are presented both visually and quantitatively.

3.B. 2D cartesian sampling of static pomelo

First, we acquired a $T1$-weighted pomelo image using a SE sequence (matrix: 256×256, res = 1×1 mm^2, 35 slices with 6 mm thickness and no gap, TR/TE = 600/8 ms, flip angle = 90°). Then, we injected a contrast agent into the pomelo in order to create structural changes in the pomelo without changing its spatial orientation. We then repeated the scan with the same acquisition parameters to obtain a postcontrast $T1$-weighted (T1c) image. As a result, we obtained two pomelo images, spatially matched, that simulate a baseline scan and a follow-up scan that consists of changes from the baseline scan.

The aim of the simulation is to examine the performance of utilizing sparsity in both the wavelet and temporal domains with adaptive sampling for longitudinal scans, with LACS-MRI, in the absence of external artifacts such as miss-registration errors or movements during acquisition.

We performed 2D reconstruction with LACS-MRI, CS-MRI, and TCS-MRI. We set the number of samples acquired at the first iteration for LACS-MRI to $N_k = 8$ lines. Results are shown with corresponding acceleration factors of 4, 6.4, and 10.6. The SER values of the different reconstruction results are shown in Table I. Figure 4 shows the baseline and follow-up pomelo images and the reconstruction results. Due to undersampling in the y-axis, we can see a recurrent artifact pattern along the y-axis which is mostly visible in the CS-MRI reconstructions. Difference images for this experiment are shown in Fig. 9 in the Appendix.

TABLE I. Comparisons of the SER (dB), pomelo experiment.

Acceleration factor	CS-MRI	TCS-MRI	LACS-MRI
10.6	2.2468	2.9052	3.6107
6.4	2.9139	7.0814	13.8731
4	4.1401	10.9464	18.2111

As expected, reconstruction results improve when the acceleration ratio decreases for all methods. The major differences between the baseline and follow-up scans consist of two enhancing regions (marked in arrows), due to the injection of a contrast agent before the acquisition of the follow-up scan. It can be seen that LACS-MRI converges to a more "uniformly" distributed sampling pattern, leading to improved reconstruction quality thanks to the adaptive sampling mechanism.

In terms of both image resolution and SER, LACS-MRI outperforms TCS-MRI and CS-MRI, by exhibiting significantly improved recovery of the image at 4-fold acceleration, which also allows to identify changes versus the baseline scans, i.e., the two enhanced areas. Although both TCS-MRI and LACS-MRI utilize temporal similarity in the reconstruction process, this experiment emphasizes the advantage of embedding weighted reconstruction and adaptive sampling. Together with the weighting mechanism, the sampling locations (shown in the bar next to each image) which were chosen adaptively by LACS-MRI lead to improved reconstruction results versus the pure random sampling used in CS-MRI and TCS-MRI.

3.C. 3D fast spoiled gradient echo brain imaging

Applying CS for 3D imaging allows undersampling in the 2D phase encode plane, thereby obtaining better performance than applying 2D CS slice by slice. We used two retrospectively undersampled scans of a patient with OPG, where scans were acquired in an interval of six months. We used contrast enhanced 3D $T1$-weighted FSPGR sequence (matrix: $512\times512\times46$, res = 0.47×0.47 mm^2, slice thickness = 1.7 mm, TI/TR/TE = 450/14.5/6.3 ms, flip angle = 20°). We rigidly registered the latter scan to the former scan and then undersampled the 3DFT trajectory with corresponding acceleration factors of 5, 10, and 16.6 (20%, 10%, and 6% of the k-space). For LACS-MRI, we begin with variable density random undersampling of 2% of the k-space and acquire additional 2% of the k-space at each iteration.

Table II shows the SER values of the different reconstruction results. Figure 5 shows the reconstruction results at 5, 10, and 16.6-fold acceleration of a patient with OPG. Both TCS-MRI and LACS-MRI exhibit almost no loss of information at 10-fold acceleration. Similar results are obtained with CS-MRI only at 5-fold acceleration. Difference images for this experiment are shown in Fig. 10 in the Appendix.

This experiment shows that thanks to the ability to undersample the 2D phase encode plane, the advantage of temporal similarity exploitation is emphasized. Therefore, LACS-MRI allows shortening the scanning time by a factor of 10, with no significant loss of information in this case.

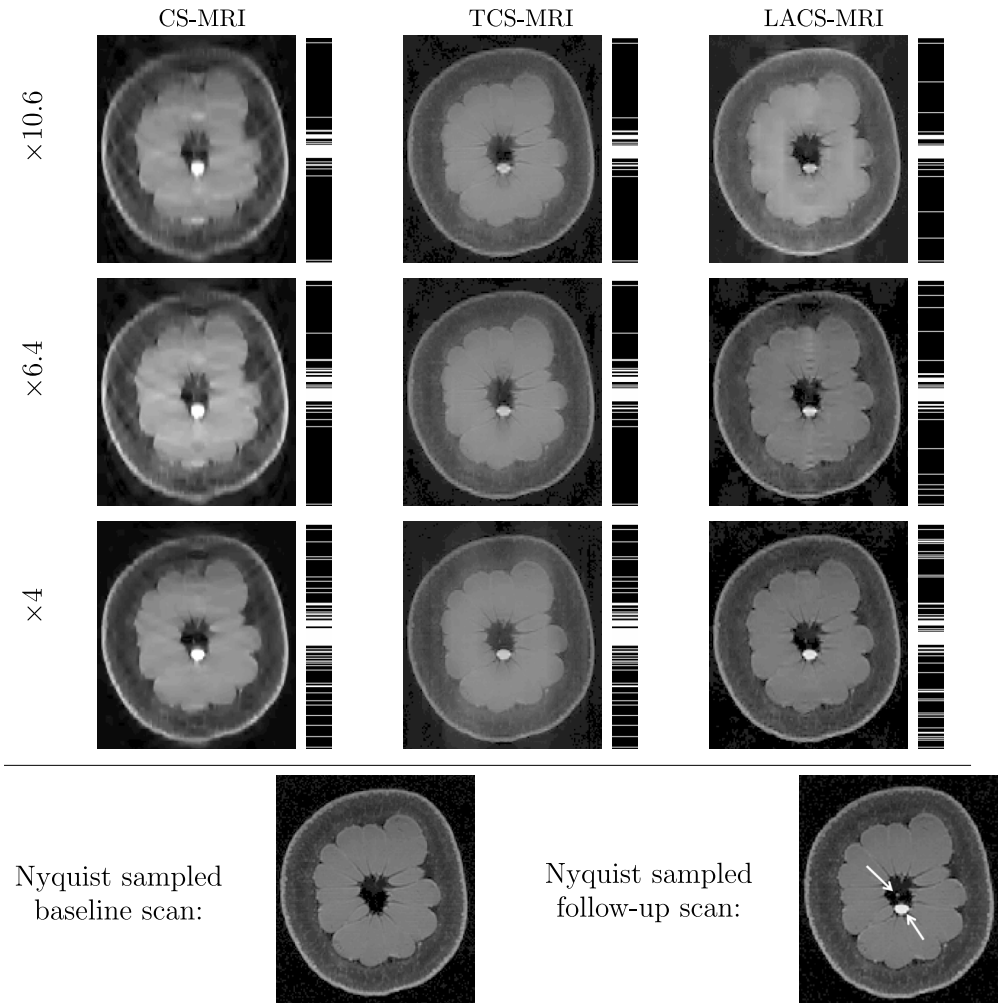

FIG. 4. Pomelo experiment: the bottom row shows the scans of a pomelo before (left) and after (right) contrast agent injection, simulating a baseline and a follow-up scan. The major changes are seen in the follow-up scan as two enhancing regions, marked by arrows on the Nyquist sampled follow-up scan. Results of CS-MRI, TCS-MRI, and LACS-MRI are presented at acceleration factors of 4, 6.4, and 10.6. The bar next to each image shows sampled phase encode lines under each scheme. It can be seen that LACS-MRI outperforms CS-MRI and TCS-MRI and exhibits significantly improved resolution at acceleration factor of 4.

3.D. 2D fast spin-echo brain imaging of rapidly changing tumor

To examine the performance of our approach with brain MRI data when the assumptions of similarity between consecutive scans are not valid, we used retrospectively acquired data of a patient with GBM. The patient was scanned twice within an interval of five months and exhibited changes between scans that occupy more than 50% of the brain region. We used $T2$-weighted FSE sequence (matrix: 512×512 res $= 0.47 \times 0.47$ mm^2, 36 slices with 4 mm thickness and no gap, TR/TE = 3500/113 ms, echo-train length = 24, flip angle = 90°). We registered the follow-up scan to the baseline scan and examined the results of LACS-MRI ($N_k = 16$), CS-MRI, and TCS-MRI with acceleration factors of 4, 6.4, and 10.6. The goal of this experiment is to validate the performance of LACS-MRI in the case of fast growing tumor, and to show that in the worst case, when the baseline scan and the follow-up scans are different, LACS-MRI does not rely on the baseline scan for reconstruction and provides results that are similar to CS-MRI.

TABLE II. Comparisons of the SER (dB), 3D FSPGR experiment.

Acceleration factor	CS-MRI	TCS-MRI	LACS-MRI
16.6	11.5093	20.4286	24.8350
10	22.9917	24.3437	27.3621
5	25.4494	28.0273	29.9281

Table III shows the SER values for different reconstructions and Fig. 6 shows reconstruction results visually, at an acceleration factor of 4 (25% of the k-space). In this case, there are major changes between the baseline and the follow-up scans due to therapy response. As a result, TCS-MRI exhibits poor performance in the vicinity of the changing tumor, since it is partially based on similarity between the consecutive scans, an assumption which is not valid in this case. LACS-MRI, however, convergences to a result which is similar to CS-MRI. This is obtained thanks to the adaptive sampling and the weighting mechanism embedded in LACS-MRI, which reduces the weight given to the similarity to prior scan in the reconstruction process, if such similarity does not exist.

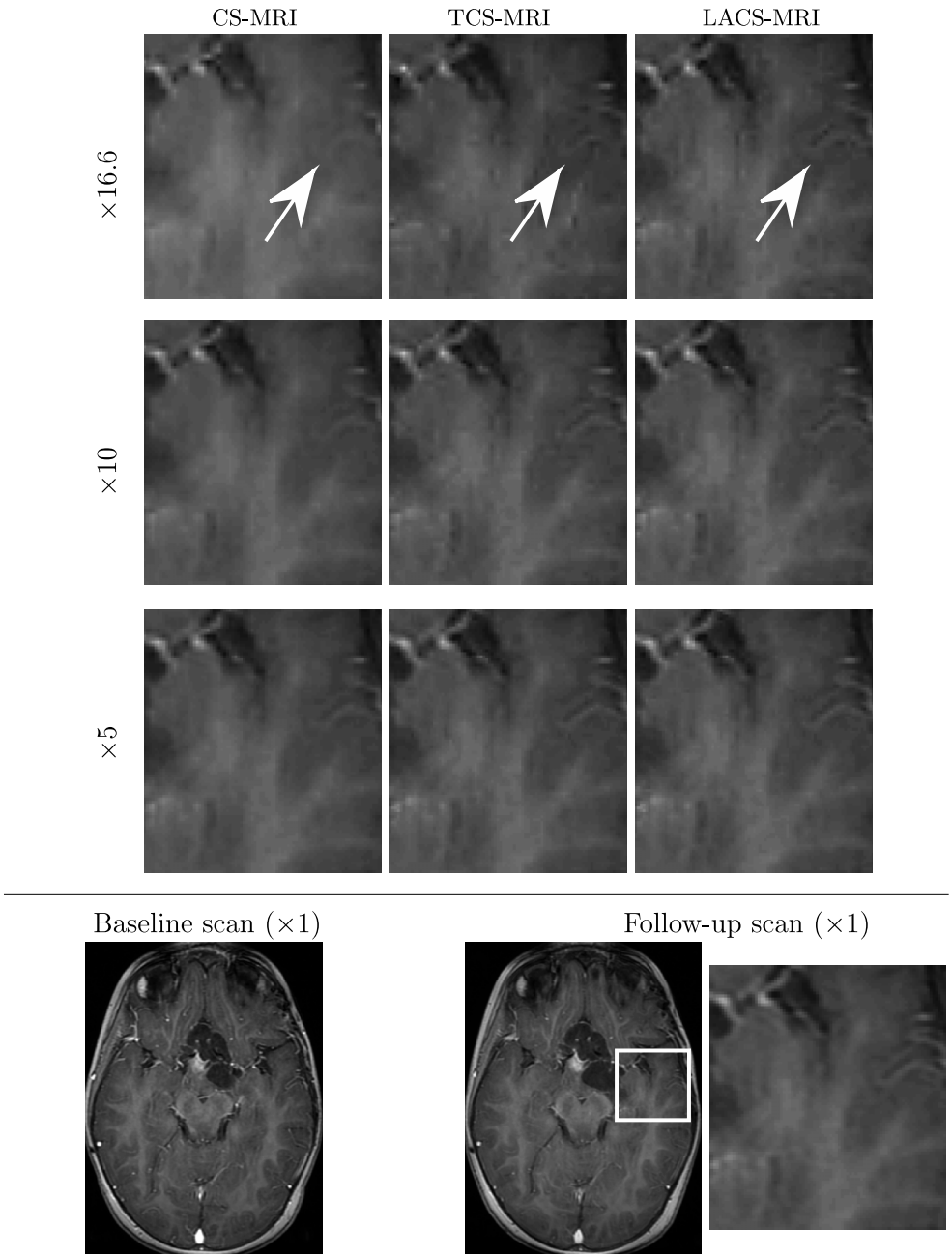

FIG. 5. 3D FSPGR results. While CS-MRI and TCS-MRI exhibit artifacts at 16.6-fold acceleration, improved resolution is obtained using LACS-MRI (pointed by arrows). At 10-fold acceleration, TCS-MRI and LACS-MRI exhibit similar satisfactory performance, while results obtained with CS-MRI include some reconstruction artifacts. At 5-fold acceleration, all methods provide almost no loss of information with slightly better performance obtained by LACS-MRI.

3.E. Sensitivity analysis

To compare the sensitivity of CS-MRI, TCS-MRI, and LACS-MRI to changes in the values of λ_1 and λ_2, we examine the SER results of each algorithm for the pomelo experiment in speed-up factor of 6.4, under various values of λ_1 and λ_2. We decided to use the pomelo experiment for this analysis since it is a static experiment that is not influenced by external additional parameters such as head motion during acquisition and different coil sensitivities.

TABLE III. Comparisons of the SER (dB), 2D FSE experiment, major temporal changes.

Acceleration factor	CS-MRI	TCS-MRI	LACS-MRI
10.6	8.2324	7.4092	8.9705
6.4	9.1760	8.2584	9.7180
4	20.1972	18.1775	20.6306

Figure 7 shows the SER results of CS-MRI as λ_1 varies, and the results of TCS-MRI and LACS-MRI for various values of λ_2 as λ_1 varies. For CS-MRI, we see that the SER results exhibit small changes around the value of 2.9 dB. In TCS-MRI and LACS-MRI, however, SER spans over a wider range of values (between 2.8 and 7.1 dB for TCS-MRI, and between 3.5 and 13.9 dB for LACS-MRI). While LACS-MRI provides better results in terms of SER, both TCS-MRI and LACS-MRI

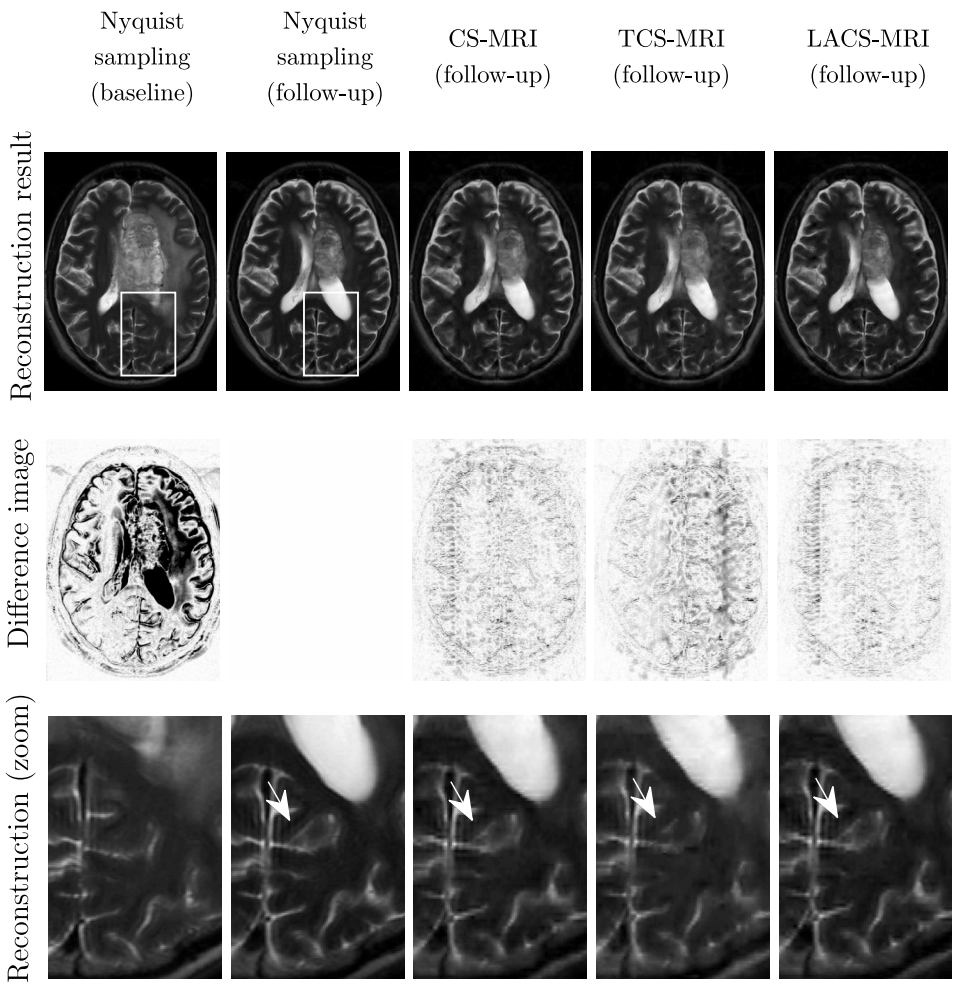

FIG. 6. 2D FSE brain imaging results when similarity between baseline and follow-up is minimal. The leftmost column shows the baseline scan used as $\mathbf{x}_0$ for TCS-MRI and LACS-MRI. The difference image between the baseline and the follow-up scans shows substantial changes due to rapid tumor changes. The last row shows an enlargement of the white rectangle. The white arrows point to a structure that has been reconstructed properly in both CS-MRI and LACS-MRI. TCS-MRI exhibits artifacts in the reconstruction of this structure due to its wrong assumption of substantial similarity between the baseline and follow-up scans.

results have a global maximum as opposed to CS-MRI that exhibits a fluctuating pattern. This allows the user to better identify the optimal parameters in TCS-MRI and LACS-MRI as opposed to CS-MRI.

Another interesting analysis is the sensitivity to λ_1 of LACS-MRI (using fixed λ_2) and CS-MRI in the case of rapidly changing tumor. Figure 8 shows the results of this sensitivity analysis. Since LACS-MRI converges to the CS-MRI solution, we see that the sensitivity patterns of both algorithms are similar, where minor differences exist due to a slightly different sampling pattern used in LACS-MRI during the convergence process.

3.F. Analysis of sources of image quality improvement

LACS-MRI includes two improvements versus TCS-MRI: adaptively determined sampling pattern and weighted image reconstruction algorithm. To appreciate the potential of the proposed methodology separating contributions from adaptive sampling and weighted reconstruction, we analyze the

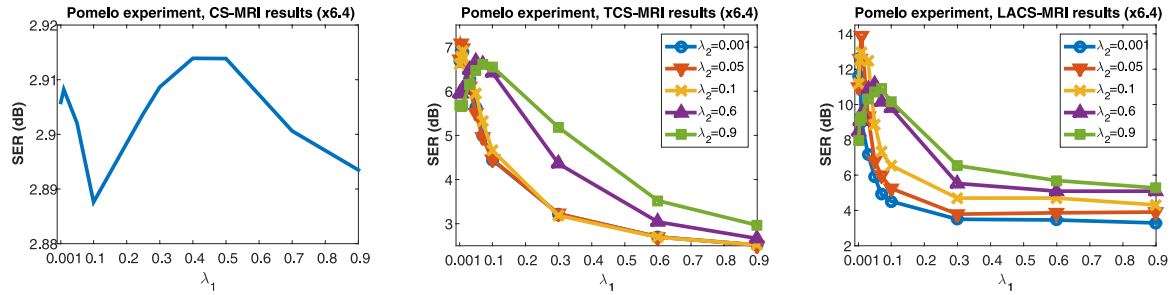

FIG. 7. Sensitivity analysis: SER results of pomelo experiment for various values of λ_1 and λ_2 for CS-MRI (left), TCS-MRI (middle), and LACS-MRI (right) methods.

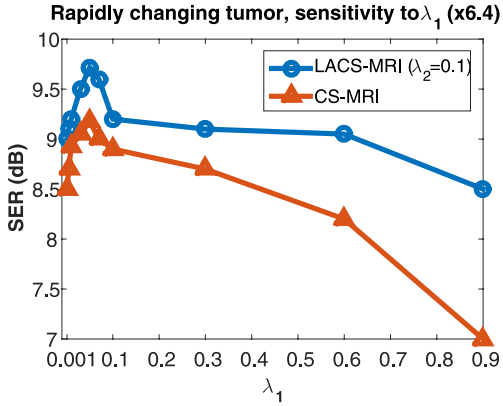

FIG. 8. Sensitivity analysis: SER results of rapidly changing tumor experiment for various values of λ_1 for CS-MRI and LACS-MRI.

contribution of the weighted mechanism solely as follows. We applied the TCS-MRI and CS-MRI algorithms using the samples obtained adaptively with LACS-MRI in the pomelo experiment. Table IV shows the SER of CS-MRI, TCS-MRI, and LACS-MRI using the samples that were taken adaptively.

When we compare the adaptive results of TCS-MRI to its nonadaptive results (Table I), we see that the adaptive scheme is responsible for approximately 30% of the improvement obtained with LACS-MRI compared to TCS-MRI, where the remaining improvement is thanks to the weighted reconstruction. This experiment shows that even when a random sampling pattern is designed such that it converges to the adaptive one for a specific scenario, LACS-MRI shows substantial improvement thanks to its weighted reconstruction.

4. DISCUSSION

4.A. Reproducing image orientation in longitudinal studies

The exploitation of temporal similarity in longitudinal studies assumes that the past scan and the follow-up scan are spatially matched. In our experiments, we worked with retrospectively acquired data and rigidly registered the latter scan to the former scan. Note that our method exhibits reliable performance even when minor registration errors exist (as can be seen in the difference images in Fig. 6), thanks to the similarity of adjacent pixels in MRI.

The practical implementation of our method for prospective acquisition of follow-up scans requires reproducing the past scan's slice positions for the scan being acquired. This spatial matching is currently offered as a feature by commercial MRI vendors[61] and is based on several anatomical landmarks. As previously noted, our method is expected to overcome minor matching errors which might be produced by these tools thanks to the fact that adjacent pixels have similar values in many MRI applications.

TABLE IV. Comparisons of the SER (dB), pomelo experiment (adaptive sampling).

Acceleration factor	CS-MRI (adaptive)	TCS-MRI (adaptive)	LACS-MRI (adaptive)
10.6	2.5678	3.186	3.6107
6.4	4.9195	9.0148	13.8731
4	6.2958	12.9328	18.2111

An additional practical solution could utilize the adaptive sampling mechanism. Partially sampled data can be used to determine the spatial orientation of the patient versus the reference image, during acquisition. This approach has been tested to compensate motions during imaging[62,63] and may be utilized for the longitudinal scanning case.

The applicability of the proposed method to other body parts such as abdominal MRI is more complicated as it may require nonrigid registration. Therefore, this paper focuses on the application of CS for longitudinal brain scans, while the implementation for regions outside of the brain is left for future research.

4.B. Gray-level intensity differences

The exploitation of temporal similarity is performed by utilizing the fact that the difference between the baseline and the follow-up scans is sparse and consists of changes in anatomy or pathology. However, changes between baseline and follow-up scans may be the result of other factors, such as acquisition parameters and field inhomogeneity. In this work, we normalized the gray-level intensity values of the scans to match the same scale, in order to minimize the effect of external factors on changes between the scans. This normalization was sufficient for producing the results presented in this paper. In prospective scanning, the normalization coefficients can be determined iteratively, during the sampling and reconstruction process.

In order to minimize the effect of external parameters on the resulted clinical follow-up, this method would work best when longitudinal scans are acquired in the same scanning site with the same scanning parameters. When the baseline and follow-up scans are acquired with different acquisition parameters on different systems, we can still exploit the structural similarity between the baseline and the follow-up scans for rapid acquisition. While this extension is not in the scope of this paper, the reader is referred to the works of Bilgic *et al.*[64] and Huang *et al.*[65] who utilize the structural similarity between various MRI sequences for rapid scanning.

4.C. Computational complexity

Fast algorithms for solving ℓ_1 minimization problems have gained much attention recently. Besides FISTA,[58] used in our experiments, we find NESTA,[57] SALSA,[66] C-SALSA,[67] and SPGL1 (Ref. 68) among other approaches that report improved convergence time and have not been explored in this work. Fast convergence time is important in our adaptive sampling approach that requires solving an ℓ_1 minimization problem to decide on the sampling locations for the next iteration. In a MATLAB (The MathWorks, Natick, MA) implementation, each ℓ_1 minimization for 256×256 brain image requires approximately 35 s.

While our implementation of FISTA at present does not attain the high rates required for solving ℓ_1 minimization for real-time applications, we expect a significant reduction in the

reconstruction time by code optimization. Moreover, recent publications have shown that GPU-based programming can significantly improve the CS based reconstruction speed from a few tens of seconds to less than one second.[69,70] In addition, during the ℓ_1 minimization computation time of a certain slice, partial data can be acquired from other 2D slices in the image to avoid "dead" time periods. Examining new approaches for ℓ_1 minimization, algorithmic simplifications, combined with massively parallel digital computation and GPU programming could allow our framework to be used for real time MRI scanning.

5. CONCLUSIONS

Repeated scans constitute a substantial portion of MRI scanning today, mainly to track changes in pathologies and to monitor treatment efficacy. We presented LACS-MRI based on adaptive sampling and weighted reconstruction for rapid MR imaging of longitudinal studies. We demonstrated experimental verification of several implementations for 2D and 3D Cartesian imaging. We showed that the temporal sparsity of longitudinal MR images can be exploited to significantly reduce scan time of follow-up scans, or alternatively, improve their resolution.

We demonstrated that unlike other CS-MRI applications, sparsity in the temporal domain is not guaranteed in longitudinal studies. We showed that our method provides almost no loss of information at 10-fold acceleration of 3D brain scans, when there is substantial similarity between baseline and follow-up scan. Moreover, our method adapts to a scenario in which there is substantial difference between the scans and results converge to state-of-the-art CS-MRI in this case.

LACS-MRI can play a major part in applications that consist of patient's disease follow-up and changes monitoring. This could be a first step toward utilizing the huge amount of data in picture archiving and communication systems (PACS) to speed-up MRI.

ACKNOWLEDGMENTS

The authors wish to thank the Gilbert Israeli Neurofibromatosis Center (GINFC) for providing the real data and supporting the medical part of the paper. This research was supported by the Ministry of Science and Technology, Israel and by the ISF I-CORE joint research center of the Technion and the Weizmann Institute, Israel.

APPENDIX: DIFFERENCE MAPS FOR POMELO AND 3D FAST SPOILED GRADIENT ECHO BRAIN IMAGING EXPERIMENTS

To appreciate superiority of the proposed LACS-MRI approach over CS-MRI and TCS-MRI, this appendix includes the difference maps of the results presented in Figs. 4 and 5. It can be seen that the difference maps obtained by LACS-MRI are less noisy than the ones provided by CS-MRI and T-CS-MRI.

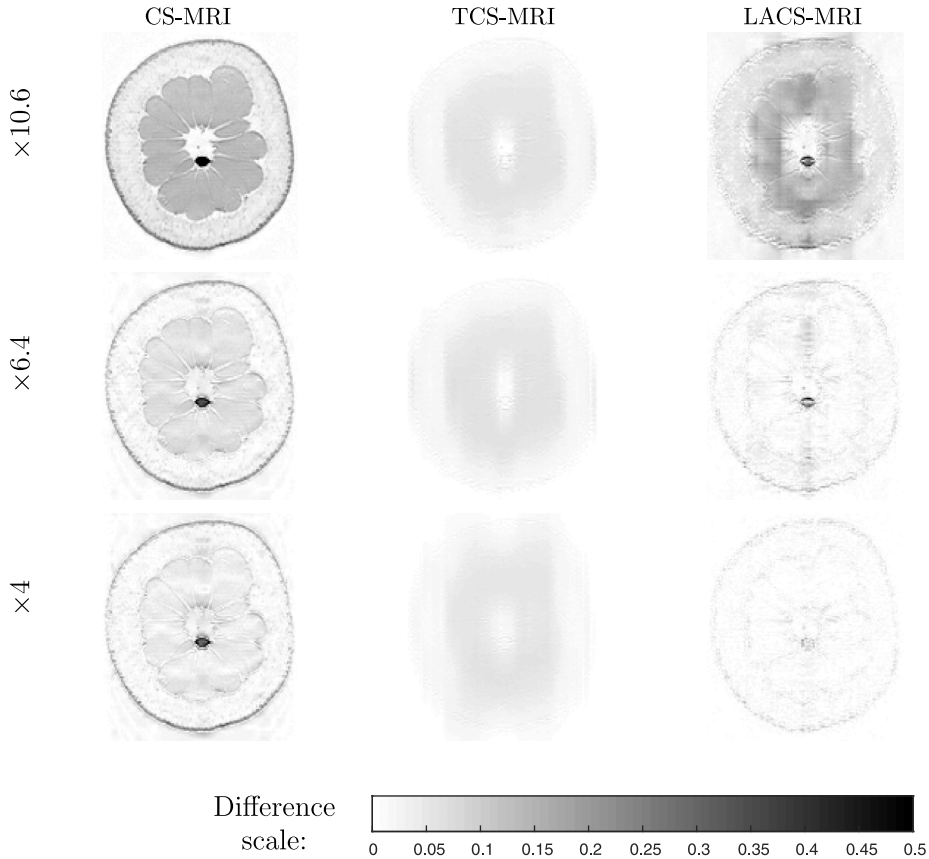

FIG. 9. Difference maps for the pomelo experiment. The absolute difference was computed after images were scaled to gray level values between 0 and 1. Reconstruction results are shown in Fig. 4.

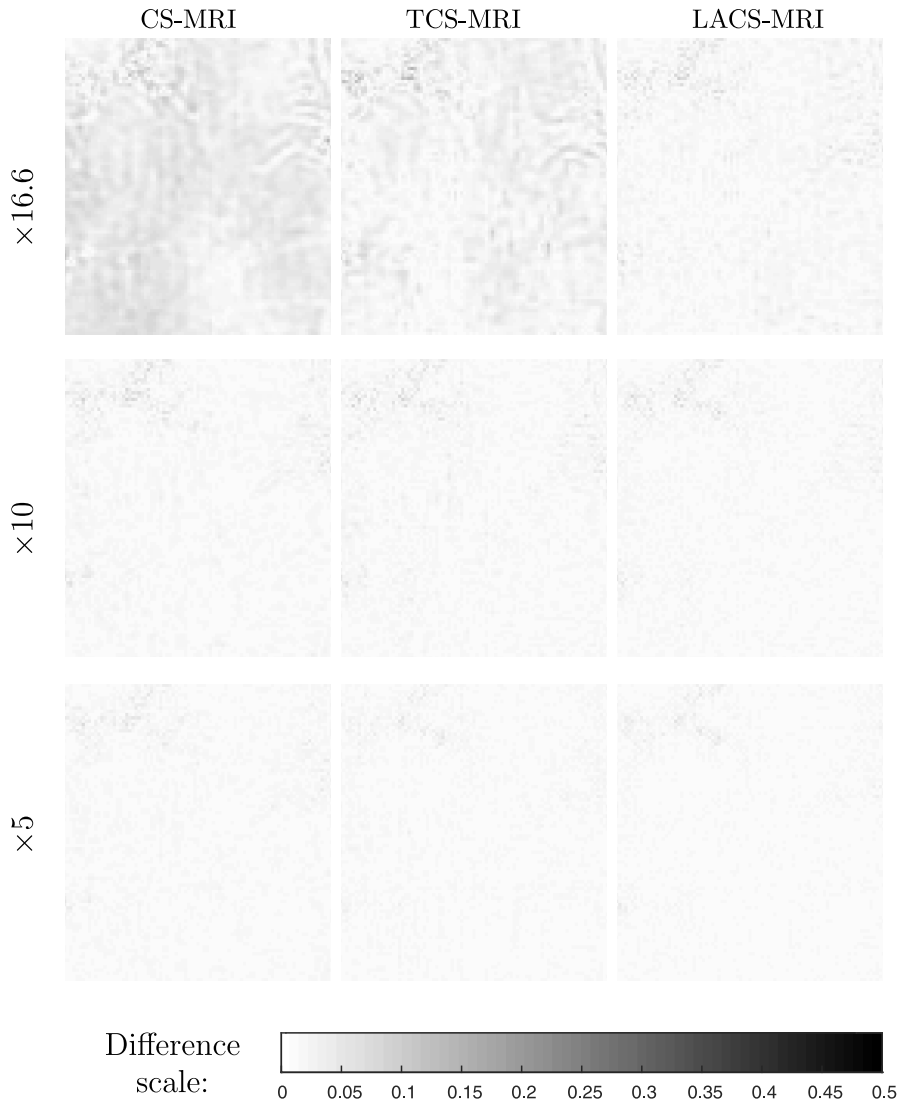

FIG. 10. Difference maps for the 3D fast spoiled gradient echo brain imaging experiment. The absolute difference was computed after images were scaled to gray level values between 0 and 1. Reconstruction results are shown in Fig. 5.

[a]Author to whom correspondence should be addressed. Electronic mail: weizmanl@tx.technion.ac.il; Telephone: +972-4-8291724.

[1]J. Rees, H. Watt, H. R. Jäger, C. Benton, D. Tozer, P. Tofts, and A. Waldman, "Volumes and growth rates of untreated adult low-grade gliomas indicate risk of early malignant transformation," Eur. J. Radiol. **72**(1), 54–64 (2009).

[2]G. S. Young, E. A. Macklin, K. Setayesh, J. D. Lawson, P. Y. Wen, A. D. Norden, J. Drappatz, and S. Kesari, "Longitudinal MRI evidence for decreased survival among periventricular glioblastoma," J. Neuro-Oncol. **104**(1), 261–269 (2011).

[3]L. Weizman, L. Ben Sira, L. Joskowicz, S. Constantini, R. Precel, B. Shofty, and D. Ben Bashat, "Automatic segmentation, internal classification, and follow-up of optic pathway gliomas in MRI," Med. Image Anal. **16**(1), 177–188 (2012).

[4]E. Yip, J. Yun, K. Wachowicz, A. A. Heikal, Z. Gabos, S. Rathee, and B. G. Fallone, "Prior data assisted compressed sensing: A novel MR imaging strategy for real time tracking of lung tumors," Med. Phys. **41**(8), 082301 (12pp.) (2014).

[5]L. Weizman, L. Ben Sira, L. Joskowicz, D. L. Rubin, K. W. Yeom, S. Constantini, B. Shofty, and D. Ben Bashat, "Semiautomatic segmentation and follow-up of multicomponent low-grade tumors in longitudinal brain MRI studies," Med. Phys. **41**(5), 052303 (14pp.) (2014).

[6]G. H. Chen, J. Tang, and S. Leng, "Prior image constrained compressed sensing (piccs) a method to accurately reconstruct dynamic CT images from highly undersampled projection data sets," Med. Phys. **35**(2), 660–663 (2008).

[7]P. Theriault Lauzier, J. Tang, and G. H. Chen, "Prior image constrained compressed sensing: Implementation and performance evaluation," Med. Phys. **39**(1), 66–80 (2012).

[8]X. Hu, D. N. Levin, P. C. Lauterbur, and T. Spraggins, "Slim: Spectral localization by imaging," Magn. Reson. Med. **8**(3), 314–322 (1988).

[9]J. J. Van Vaals, M. E. Brummer, W. Thomas Dixon, H. H. Tuithof, H. Engels, R. C. Nelson, B. M. Gerety, J. L. Chezmar, and J. A. Den Boer, "Keyhole method for accelerating imaging of contrast agent uptake," J. Magn. Reson. Imaging **3**(4), 671–675 (1993).

[10]R. A. Jones, O. Haraldseth, T. B. Müller, P. A. Rinck, and A. N. Øksendal, "K-space substitution: A novel dynamic imaging technique," Magn. Reson. Med. **29**(6), 830–834 (1993).

[11]Z. Liang and P. C. Lauterbur, "An efficient method for dynamic magnetic resonance imaging," IEEE Trans. Med. Imaging **13**(4), 677–686 (1994).

[12]F. R. Korosec, R. Frayne, T. M. Grist, and C. A. Mistretta, "Time-resolved contrast-enhanced 3D MR angiography," Magn. Reson. Med. **36**(3), 345–351 (1996).

[13]B. Madore, G. H. Glover, and N. J. Pelc, "Unaliasing by Fourier-encoding the overlaps using the temporal dimension (UNFOLD), applied to cardiac imaging and fMRI," Magn. Reson. Med. **42**(5), 813–828 (1999).

[14]J. Tsao, P. Boesiger, and K. P. Pruessmann, "k-t BLAST and k-t sense: Dynamic MRI with high frame rate exploiting spatiotemporal correlations," Magn. Reson. Med. **50**(5), 1031–1042 (2003).

[15]C. A. Mistretta, O. Wieben, J. Velikina, W. Block, J. Perry, Y. Wu, and K. Johnson, "Highly constrained backprojection for time-resolved MRI," Magn. Reson. Med. **55**(1), 30–40 (2006).
[16]Y. Cao, D. N. Levin, and L. Yao, "Locally focused MRI," Magn. Reson. Med. **34**(6), 858–867 (1995).
[17]Y. Cao and D. N. Levin, "Feature-recognizing MRI," Magn. Reson. Med. **30**(3), 305–317 (1993).
[18]E. J. Candès, "Compressive sampling," in *Proceedings of the International Congress of Mathematicians: Madrid, August 22-30, 2006: Invited Lectures* (EMS Publishing House, Zürich, Switzerland, 2006), pp. 1433–1452.
[19]D. L. Donoho, "Compressed sensing," IEEE Trans. Inf. Theory **52**(4), 1289–1306 (2006).
[20]Y. C. Eldar and G. Kutyniok, *Compressed Sensing: Theory and Applications* (Cambridge University Press, Cambridge, UK, 2012).
[21]Y. C. Eldar, *Sampling Theory: Beyond Bandlimited Systems* (Cambridge University Press, Cambridge, UK, 2014).
[22]M. Lustig, D. Donoho, and J. M. Pauly, "Sparse MRI: The application of compressed sensing for rapid MR imaging," Magn. Reson. Med. **58**(6), 1182–1195 (2007).
[23]U. Gamper, P. Boesiger, and S. Kozerke, "Compressed sensing in dynamic MRI," Magn. Reson. Med. **59**(2), 365–373 (2008).
[24]D. Liang, E. V. R. DiBella, R. Chen, and L. Ying, "k-t ISD: Dynamic cardiac MR imaging using compressed sensing with iterative support detection," Magn. Reson. Med. **68**(1), 41–53 (2012).
[25]D. Zonoobi and A. A. Kassim, "On the reconstruction of sequences of sparse signals–the weighted-cs," J. Visual Commun. Image Representation **24**(2), 196–202 (2013).
[26]J. D. Trzasko, C. R. Haider, E. A. Borisch, N. G. Campeau, J. F. Glockner, S. J. Riederer, and A. Manduca, "Sparse-capr: Highly accelerated 4d CE-MRA with parallel imaging and nonconvex compressive sensing," Magn. Reson. Med. **66**(4), 1019–1032 (2011).
[27]H. Wu, W. F. Block, and A. A. Samsonov, "Hypr-constrained compressed sensing reconstruction for accelerated time resolved imaging," in *Proceedings of the 16th Annual Meeting of ISMRM, Toronto, Canada* (International Society for Magnetic Resonance in Medicine, Berkeley, CA, 2008), p. 339.
[28]A. A. Samsonov, J. V. Velikina, J. O. Fleming, M. L. Schiebler, and A. S. Field, "Accelerated serial MR imaging in multiple sclerosis using baseline scan information," in *Proceedings of the 18th Annual Meeting of ISMRM, Stockholm, Sweden* (International Society for Magnetic Resonance in Medicine, Berkeley, CA, 2010), p. 4876.
[29]C. Tsai and D. G. Nishimura, "Reduced aliasing artifacts using variable-density k-space sampling trajectories," Magn. Reson. Med. **43**(3), 452–458 (2000).
[30]F. Knoll, C. Clason, C. Diwoky, and R. Stollberger, "Adapted random sampling patterns for accelerated MRI," Magn. Reson. Mater. Phys., Biol. Med. **24**(1), 43–50 (2011).
[31]L. P. Panych and F. A. Jolesz, "A dynamically adaptive imaging algorithm for wavelet-encoded MRI," Magn. Reson. Med. **32**(6), 738–748 (1994).
[32]S. S. Yoo, C. R. G. Guttmann, L. Zhao, and L. P. Panych, "Real-time adaptive functional MRI," Neuroimage **10**(5), 596–606 (1999).
[33]M. Seeger, H. Nickisch, R. Pohmann, and B. Schölkopf, "Optimization of k-space trajectories for compressed sensing by Bayesian experimental design," Magn. Reson. Med. **63**(1), 116–126 (2010).
[34]S. Ravishankar and Y. Bresler, "Adaptive sampling design for compressed sensing MRI," in *2011 Annual International Conference of the IEEE Engineering in Medicine and Biology Society, EMBC* (IEEE, NJ, 2011), pp. 3751–3755.
[35]S. Ravishankar and Y. Bresler, "MR image reconstruction from highly undersampled k-space data by dictionary learning," IEEE Trans. Med. Imaging **30**(5), 1028–1041 (2011).
[36]J. Haupt, R. M. Castro, and R. Nowak, "Distilled sensing: Adaptive sampling for sparse detection and estimation," IEEE Trans. Inf. Theory **57**(9), 6222–6235 (2011).
[37]D. Wei and A. O. Hero, "Multistage adaptive estimation of sparse signals," IEEE J. Sel. Top. Signal Process. **7**(5), 783–796 (2013).
[38]Y. Chen, S. Bhojanapalli, S. Sanghavi, and R. Ward, "Completing any low-rank matrix, provably," preprint arXiv:1306.2979, 2014.
[39]E. J. Candes, M. B. Wakin, and S. P. Boyd, "Enhancing sparsity by reweighted l1 minimization," J. Fourier Anal. Appl. **14**(5-6), 877–905 (2008).
[40]J. P. Haldar, D. Hernando, S. K. Song, and Z. P. Liang, "Anatomically constrained reconstruction from noisy data," Magn. Reson. Med. **59**(4), 810–818 (2008).
[41]N. Vaswani and W. Lu, "Modified-cs: Modifying compressive sensing for problems with partially known support," IEEE Trans. Signal Process. **58**(9), 4595–4607 (2010).
[42]T. Lang and J. Ji, "Accelerating dynamic contrast-enhanced MRI using compressed sensing," in *Proceedings of the 16th Annual Meeting of ISMRM, Toronto, Canada* (International Society for Magnetic Resonance in Medicine, Berkeley, CA, 2008), p. 1481.
[43]H. Jung, K. Sung, K. S. Nayak, E. Y. Kim, and J. C. Ye, "k-t focuss: A general compressed sensing framework for high resolution dynamic MRI," Magn. Reson. Med. **61**(1), 103–116 (2009).
[44]M. Lustig, J. M. Santos, D. L. Donoho, and J. M. Pauly, "kt sparse: High frame rate dynamic MRI exploiting spatio-temporal sparsity," in *Proceedings of the 13th Annual Meeting of ISMRM* (International Society for Magnetic Resonance in Medicine, Seattle, 2006), Vol. 2420.
[45]I. Daubechies *et al.*, in *Ten Lectures on Wavelets* Vol. 61 (SIAM, PA, 1992).
[46]J. A. Fessler, N. H. Clinthorne, and W. L. Rogers, "Regularized emission image reconstruction using imperfect side information," IEEE Trans. Nucl. Sci. **39**(5), 1464–1471 (1992).
[47]A. O. Hero, R. Piramuthu, J. A. Fessler, and S. R. Titus, "Minimax emission computed tomography using high-resolution anatomical side information and b-spline models," IEEE Trans. Inf. Theory **45**(3), 920–938 (1999).
[48]M. A. Khajehnejad, W. Xu, A. S. Avestimehr, and B. Hassibi, "Weighted 1 minimization for sparse recovery with prior information," in *IEEE International Symposium on Information Theory, ISIT* (IEEE, NJ, 2009), pp. 483–487.
[49]M. P. Friedlander, H. Mansour, R. Saab, and Ö. Yilmaz, "Recovering compressively sampled signals using partial support information," IEEE Trans. Inf. Theory **58**(2), 1122–1134 (2012).
[50]D. Zonoobi and A. A. Kassim, "Weighted-cs for reconstruction of highly under-sampled dynamic MRI sequences," in *Signal Information Processing Association Annual Summit and Conference (APSIPA ASC), 2012 Asia-Pacific* (IEEE, NJ, 2012), pp. 1–5.
[51]G. P. Zientara, L. P. Panych, and F. A. Jolesz, "Dynamically adaptive MRI with encoding by singular value decomposition," Magn. Reson. Med. **32**(2), 268–274 (1994).
[52]S. K. Nagle and D. N. Levin, "Multiple region MRI," Magn. Reson. Med. **41**(4), 774–786 (1999).
[53]Y. Gao and S. J. Reeves, "Optimal k-space sampling in MRSI for images with a limited region of support," IEEE Trans. Med. Imaging **19**(12), 1168–1178 (2000).
[54]J. Haupt, R. Nowak, and R. Castro, "Adaptive sensing for sparse signal recovery," in *IEEE 13th Digital Signal Processing Workshop and 5th IEEE Signal Processing Education Workshop, DSP/SPE* (IEEE, NJ, 2009), pp. 702–707.
[55]E. Arias-Castro, E. J. Candes, and M. A. Davenport, "On the fundamental limits of adaptive sensing," IEEE Trans. Inf. Theory **59**(1), 472–481 (2013).
[56]D. L. Donoho and Y. Tsaig, "Fast solution of-norm minimization problems when the solution may be sparse," IEEE Trans. Inf. Theory **54**(11), 4789–4812 (2008).
[57]S. Becker, J. Bobin, and E. J. Candès, "Nesta: A fast and accurate first-order method for sparse recovery," SIAM J. Imaging Sci. **4**(1), 1–39 (2011).
[58]A. Beck and M. Teboulle, "A fast iterative shrinkage-thresholding algorithm for linear inverse problems," SIAM J. Imaging Sci. **2**(1), 183–202 (2009).
[59]L. Weizman, Y. C. Eldar, and D. Ben Bashat, "The application of compressed sensing for longitudinal MRI," preprint arXiv:1407.2602, 2014.
[60]Y. Tsaig and D. L. Donoho, "Extensions of compressed sensing," Signal Process. **86**(3), 549–571 (2006).
[61]K. McMillan, M. Uike, X. Tao, S. Kosugi, and H. Okuda, "MR efficiency becomes critical as healthcare costs, scanner time demand increases," in *Signa Pulse of MRI* (Autumn, Buckinghamshire, UK, 2010), pp. S10–S13.
[62]S. G. Lingala, M. Nadar, C. Chefd'Hotel, L. Zhang, and M. Jacob, "Unified reconstruction and motion estimation in cardiac perfusion MRI," in *IEEE International Symposium on Biomedical Imaging: From Nano to Macro* (IEEE, NJ, 2011), pp. 65–68.
[63]L. Feng, R. Grimm, K. T. Block, H. Chandarana, S. Kim, J. Xu, L. Axel, D. K. Sodickson, and R. Otazo, "Golden-angle radial sparse parallel MRI: Combination of compressed sensing, parallel imaging, and golden-angle

radial sampling for fast and flexible dynamic volumetric MRI," Magn. Reson. Med. **72**, 707–717 (2013).
[64]B. Bilgic, V. K. Goyal, and E. Adalsteinsson, "Multi-contrast reconstruction with Bayesian compressed sensing," Magn. Reson. Med. **66**(6), 1601–1615 (2011).
[65]J. Huang, C. Chen, and L. Axel, "Fast multi-contrast MRI reconstruction," in *Medical Image Computing and Computer-Assisted Intervention–MICCAI 2012* (Springer, New York, NY, 2012), pp. 281–288.
[66]M. V. Afonso, J. M. Bioucas-Dias, and M. A. T. Figueiredo, "Fast image recovery using variable splitting and constrained optimization," IEEE Trans. Image Process. **19**(9), 2345–2356 (2010).
[67]M. V. Afonso, J. M. Bioucas-Dias, and M. A. T. Figueiredo, "An augmented Lagrangian approach to the constrained optimization formulation of imaging inverse problems," IEEE Trans. Image Process. **20**(3), 681–695 (2011).
[68]E. Van Den Berg and M. P. Friedlander, "Probing the Pareto frontier for basis pursuit solutions," SIAM J. Sci. Comput. **31**(2), 890–912 (2008).
[69]J. D. Blanchard and J. Tanner, "Gpu accelerated greedy algorithms for compressed sensing," Math. Prog. Comput. **5**(3), 267–304 (2013).
[70]M. Birk, R. Dapp, N. V. Ruiter, and J. Becker, "Gpu-based iterative transmission reconstruction in 3d ultrasound computer tomography," J. Parallel Distrib. Comput. **74**(1), 1730–1743 (2014).